Manuscript review amt-2020-166 « Improvement of numerical weather prediction model analysis during fog conditions through the assimilation of ground-based microwave radiometer observations: a 1D-Var study ».

First of all, the authors thank the two anonymous reviewers and the editor for their positive feedback on this new version which allows the publication with minor reviews.
All the suggested modifications have been taken into account and are highlighted in red in the marked-up manuscrit.

Improvement of numerical weather prediction model analysis during fog conditions through the assimilation of ground-based microwave radiometer observations: a 1D-Var study.

Pauline Martinet[a], Domenico Cimini[b], Frédéric Burnet[a], Benjamin Ménétrier[a], Yann Michel[a], and Vinciane Unger[a]

[a]CNRM, Université de Toulouse, Météo-France, CNRS, Toulouse, France
[b]IMAA-CNR, Potenza, Italy

Correspondence: Pauline Martinet (pauline.martinet@meteo.fr)

Abstract. This paper investigates the potential benefit of ground-based microwave radiometers (MWRs) to improve the initial state (analysis) of current numerical weather prediction (NWP) systems during fog conditions. To this end, temperature, humidity and liquid water path (LWP) retrievals have been performed by directly assimilating ~~brighness~~ brightness temperatures using a one-dimensional variational technique (1D-Var). This study focuses on a fog dedicated field-experiment performed over winter 2016-2017 in France. In-situ measurements from a 120 m tower and radiosoundings are used to assess the improvement brought by the 1D-Var analysis to the background. A sensitivity study demonstrates the importance of the cross-correlations between temperature and specific humidity in the background-error-covariance matrix as well as the bias-correction applied on MWR raw measurements. With the optimal 1D-Var configuration, a root-mean-square-error smaller than 1.5 K (~~resp.~~ respectively 0.8 K) for temperature and 1 g.kg^{-1} (~~resp.~~ respectively 0.5 g.kg^{-1}) for humidity is obtained up to 6 km altitude (~~resp.~~ respectively within the fog layer up to 250 m). A thin-radiative fog case study has shown that the assimilation of MWR observations was able to correct large temperature errors of the AROME model as well as vertical and temporal errors observed in the fog lifecycle. A statistical evaluation through the whole period has demonstrated that the largest impact when assimilating MWR observations is obtained on the temperature and LWP fields, while it is neutral to slightly positive for the specific humidity. Most of the temperature improvement is observed during false alarms when the AROME forecasts tend to significantly overestimate the temperature cooling. During missed fog profiles, 1D-Var analyses were found to increase the atmospheric stability within the first 100 m above the surface compared to the initial background profile. Concerning the LWP, the RMSE with respect to MWR statistical regressions is decreased from 101 g.m^{-2} in the background to 27 g.m^{-2} in the 1D-Var analysis. These encouraging results led to the deployment of 8 MWRs during the international SOFOG3D (SOuth FOGs 3D experiment for fog processes study) experiment conducted by Météo-France.

1 Introduction

Each year large human and economical losses are due to fog episodes, which, by the large reduction of visibility, affect aviation, marine, and land transportation ~~(Gultepe et al. (2007))~~(Gultepe et al., 2007). Fog forecasts remain quite inaccurate due to the complexity, non linearities and fine scale of the physical processes taking part in the fog lifecycle. Fog results from

a combination of radiative, turbulent and microphysical processes as well as interactions with surface heterogeneities which will drive the relative importance of local and large-scale circulations. Recently, three dimensional models have replaced one-dimensional models to forecast fog in most national weather services. Currently, convective-scale numerical weather prediction (NWP) models run with an horizontal resolution of approximately one kilometre with frequent data assimilation cycles. While the importance of vertical resolution ~~(Philip et al. (2016))~~(Philip et al., 2016), aerosol activation ~~(Mazoyer et al. (2019)~~

~~)~~ (Mazoyer et al., 2019) or water deposition ~~(Tav et al. (2018))~~ (Tav et al., 2018) have recently been highlighted to improve fog forecasts, fog is also known to be highly sensitive to initial conditions ~~(Bergot and Guedalia (1994), Bergot et al. (2005),~~ ~~Hu et al. (2014))~~(Bergot and Guedalia, 1994; Bergot et al., 2005; Hu et al., 2014). Therefore, accurate initial temperature, humidity and wind profiles are crucial to successfully forecast fog. However, the atmospheric boundary layer (ABL) has also been identified as a part of the atmosphere which is undersampled by observations. Even though satellite data ~~provide a~~

enable global coverage all over the world, they provide limited information on the ABL due to the attenuation by clouds and degraded vertical resolution in the ABL. Additionally, uncertainties in surface properties (such as skin temperature and emissivity~~, Guedj et al. (2011))~~) limit the assimilation of surface-sensitive channels over lands (Guedj et al., 2011). Recently, an Observing System Simulation Experiment (OSSE) by Hu et al. (2017), has demonstrated that temperature and moisture at the surface have a larger impact on fog forecast than surface wind observations concluding that temperature and humidity

profilers could potentially play a major role in the improvement of fog forecast initialization. Ground-based microwave radiometers (MWR) are robust instruments providing continuous observations of temperature and humidity profiles as well as integrated liquid and water contents during all-sky weather conditions. Even if their vertical resolution degrades with altitude ~~(Cimini et al. (2006))~~(Cimini et al., 2006), most of their information content resides in the ABL ~~(Löhnert and Maier (2012))~~ (Löhnert and Maier, 2012) and their high temporal resolution (few minutes) makes them suitable to monitor the evolution of

fog~~development~~. Despite the potential impact of MWRs in NWP models, assimilation experiments of their data have been limited to few attempts. The first preliminary study of Vandenberghe and Ware (2002) has demonstrated a positive impact of the assimilation of a single MWR unit into the 10 km horizontal resolution MM5 (https://www2.mmm.ucar.edu/mm5/) mesoscale model in the context of a winter fog event. The impact of a simulated network of 140 MWRs through an OSSE was also investigated by Otkin et al. (2011) and Hartung et al. (2011) on a winter storm case. This study confirmed a positive impact

on temperature and humidity analyses as well as up to 12 hour forecasts on moisture flux. More recently, a real network of 13 MWRs was assimilated by Caumont et al. (2016) into the 2.5 km horizontal resolution convective scale model AROME in the context of heavy-precipitation events in the western Mediterranean. Impact of this network was found to be neutral on temperature and humidity fields but positive on quantitative precipitation forecasts up to 18 hours. In addition, Martinet et al. (2015) and Martinet et al. (2017) have demonstrated the positive impact that could be expected on NWP temperature profile analyses

by the direct assimilation of MWR brightness temperatures into the AROME model with a one-dimensional variational framework (1D-Var). All these studies showed an encouraging positive impact of the assimilation of ~~MWRs~~ MWR observations into NWP, though they are limited to deep-convection, single case studies on low resolution limited area models, or restricted to temperature analyses only. The purpose of this article is to evaluate the expected benefit of MWRs on km-scale NWP analyses during fog events on an extended dataset over a six-month fog experiment. This expands the studies of Martinet et al. (2015) and Martinet et al. (2017) to humidity and liquid water path retrievals and evaluates the impact of new tools developed to optimize the assimilation of MWRs during COST actions TOPROF ~~(Illingworth et al. (2019)) and PROBE (Cimini et al. (2020))~~ (Illingworth et al., 2019) and PROBE (Cimini et al., 2020). A fog dedicated field experiment was carried out in the North-East of France during the winter 2016-2017 during which a 14-channel MWR has been operated. The impact of MWR brightness temperatures on temperature, humidity and liquid water content profiles forecast by AROME has been evaluated during the six-month period against in-situ data collected during intensive observation periods (IOPs) and continuous measurements deployed on a 120 m instrumented tower. This paper begins with an overview of the dataset, the AROME model and a description of the 1D-Var settings in section 2. A sensitivity study of the 1D-Var retrievals to the background-error-covariance matrix and bias-correction to select the optimal configuration is presented in section 3. Section 4 presents a case study of the first IOP showing large AROME errors during a thin radiative fog event ~~well corrected by~~ that are corrected when using the 1D-Var retrieval. Section 5 generalizes the results obtained in section 4 through a statistical evaluation of 1D-Var retrieval errors and expected impact on the AROME analyses. Section 6 presents the deployment of a regional-scale MWR network for fog forecast improvement as continuity of this study, while finally section 7 summarises the main conclusions.

2 Dataset and methodology

2.1 Instrumentation

Data sampled during a field experiment dedicated to fog process studies carried out at the ANDRA (the French National Radioactive Waste Management Agency) atmospheric platform located in Houdelaincourt (48.5623N; 5.5055E) in the North-East of France during the winter 2016-2017 are used in this study. The experimental site was chosen due to the high occurence of fogs and the possibility to take advantage of a 120 m instrumented tower. A large range of in-situ instrumentation was deployed during the six-month experiment: visibility sensors, liquid water content and droplet size distribution measurements, temperature and relative humidity measurements at different levels above ground (10 m, 50 m, 120 m). In addition to in-situ measurements, a 14-channel HATPRO MWR ~~(Rose et al. (2005))~~ (Rose et al., 2005) manufactured by Radiometer Physics Gmbh (RPG) was deployed on site during the experiment. The HATPRO MWR is a passive instrument measuring the naturally emitted downwelling radiance in two spectral ranges: 22.24 to 31 GHz to retrieve humidity profiles with a low resolution but high accurate integrated water contents (IWV) and liquid water path (LWP)~~. The~~; 51 to 58 GHz range, located in the 60 GHz O_2 absorption complex line, ~~is used~~ to retrieve temperature profiles. Elevation scans from 5.4° to 90° were used to improve the vertical resolution of temperature profiles assuming that horizontal homogeneity in the vicinity of the instrument is respected. A ceilometer Vaisala CL31 was deployed during October to December 2016 replaced by a Vaisala CT25K from January to

April 2017 to determine the cloud base altitude. In addition, 21 VAISALA RS92 radiosondes with an expected accuracy of 0.5 K in temperature and 5 % in relative humidity were launched during IOPs. Tethered balloon measurements were also carried out with the deployment of a cloud particle probe and a turbulence probe.

2.2 The AROME NWP model

In this study 1-hour forecasts from the French convective scale model AROME (Application of Research to Operations at MEsoscale, ~~Seity et al. (2011)~~Seity et al. (2011)) are used as *a priori* profiles or "backgrounds". AROME is a limited area model covering Western Europe with non-hydrostatic dynamical core. Since beginning 2015, the horizontal resolution of AROME has been increased from 2.5 km to 1.3 km as well as the number of vertical levels from 60 to 90 ~~(Brousseau et al. (2016))~~(Brousseau et al., 2016). Vertical levels follow the terrain in the lowest layers and isobars in the upper atmosphere. The detailed physics of Arome are inherited from the research Meso-NH model ~~(Lafore et al. (1997))~~(Lafore et al., 1997). Deep convection is assumed to be resolved explicitly, but shallow convection is parameterized following ~~Pergaud et al. (2009)~~Pergaud et al. (2009). A bulk one-moment microphysical scheme ~~(Pinty and Jabouille (1998))~~(Pinty and Jabouille, 1998) governs the equations of the specific contents of six water species (humidity, cloud liquid water, precipitating liquid water, pristine ice, snow, and graupel). This new version also performs 3D-Var analyses every hour instead of every three hours to optimize the use of frequent observations. All conventional observations are assimilated together with wind profilers, winds from spaceborne measurements (Atmospheric Motion Vectors and scatterometers), Doppler winds ~~(Montmerle and Faccani (2009)) and reflectivity (Wattrelot et al. (2014))~~(Montmerle and Faccani, 2009) and reflectivity (Wattrelot et al., 2014) from ground-based weather radars, satellite radiances as well as ground-based GPS measurements ~~(Mahfouf et al. (2015))~~(Mahfouf et al., 2015).

2.3 1D-Var framework

To retrieve temperature and humidity profiles and evaluate the impact on AROME analyses, a 1D-Var framework similar to the one described in Martinet et al. (2017) is used. Based on the optimal estimation theory by ~~Rodgers (2000)~~Rodgers (2000), MWR observations are optimally combined with an *a priori* estimation of the atmospheric state which, in this study, refers to 1-hour AROME forecasts. To this end, the two sources of information are weighted by their corresponding uncertainty called the background-error-covariance matrix (**B**) for the *a priori* profile and the observation-error-covariance matrix (**R**) for the observation to find the optimal state. In order to find the optimal state minimizing the distance to the observation, a radiative transfer model is needed to compute the equivalent observation from the *a priori*. The method iteratively modifies the state vector x from the *a priori* x_b to minimize the following cost function:

$$J(\mathbf{x}) = \frac{1}{2}(\mathbf{x} - \mathbf{x}_b)^{\mathrm{T}}\mathbf{B}^{-1}(\mathbf{x} - \mathbf{x}_b) + \frac{1}{2}(\mathbf{y} - \mathrm{H}(\mathbf{x}))^{\mathrm{T}}\mathbf{R}^{-1}(\mathbf{y} - \mathrm{H}(\mathbf{x}))$$

where H represents the observation operator (radiative transfer model and interpolations from model space to observation space), $^{\mathrm{T}}$ represents the transpose operator and $^{-1}$ the inverse operator. The observation-error-covariance matrix **R** should

4

take into account representativeness and forward model errors as well as radiometric noise. Throughout the manuscript, the
atmospheric state minimizing the cost function is called the "analysis" (x_a), "increment" refers to the difference between the *a priori* x_b and the analysis, "innovation" refers to the difference between the observation and the *a priori* x_b.

For the first time, the fast radiative transfer model RTTOV-gb ~~(De Angelis et al. (2016), Cimini et al. (2019)),~~ (De Angelis et al., 2016; Cim , developed specifically to simulate MWR observations for operational applications during the Cost action TOPROF, is used within the 1D-Var package maintained by the NWP Satellite Application Facility (https://www.nwpsaf.eu/site/software/1d-var/). To this end, the 1D-Var has been adapted to the ground-based sensing configuration of MWRs and interfaced with RTTOV-gb. In this study the control vector x consists in temperature and the natural logarithm of specific humidity on the same 90 levels as defined in AROME. These levels cover the atmospheric range from the ground up to 30 km, the vertical resolution decreasing with altitude: 20-100 m below 1 km, 100-200 m from 1 to 5 km, around 400 m at 10 km. Additionally to temperature and humidity, the liquid water path is also included in the control vector. Following the current implementation of the NWPSAF 1D-Var, no correlation between the LWP and the other variables is assumed in the **B** matrix. The observation vector y consists of brightness temperatures (BT) in all K-band ([1]) and V-band channels ([2]) at zenith and only opaque channels (above 54 GHz) at low elevation angles: 42°, 30°, 19.2°, 10.2° and 5.4 °. Transparent channels are not used at low elevation angles due to the violation of the assumption of horizontal homogeneity.

3 Evaluation of 1D-Var retrievals

3.1 Background errors

In variational data assimilation (either 1D-Var or 3D/4D-Var), the accuracy of the analysis will depend on the background-error covariance matrix **B**. This matrix specifies how much weight is given to the *a priori* profile compared to the observation, how the information from the localized observation is spread in the model space both vertically and horizontally (for 3D/4D-Var assimilation) and impose the balance between the model control variables. However, due to difficulties in measuring the "true" state, this **B** matrix has to be modelled. Currently, climatological, spatially homogeneous and isotropic background-error covariances are used operationally in the AROME model ~~(Brousseau et al. (2011))~~ (Brousseau et al., 2011). They are computed from 3h range forecast differences from an ensemble data assimilation over long time periods and the whole model domain. As demonstrated by Ménétrier and Montmerle (2011), climatological covariances are inadequate for fog areas which exhibit a much stronger positive coupling between temperature and humidity and attenuated vertical correlations above the fog layer.

For this study, a similar approach as the one described in Ménétrier and Montmerle (2011) has thus been used to infer background-error covariances adapted to fog layers and to the AROME configuration and the time period of the experiment. To this end, the AROME ensemble data assimilation schemes (AROME EDA) that mimics in a variational context the approach taken in the stochastic Ensemble Kalman Filter ~~(Evensen (2003))~~ (Evensen, 2003) has been used. The EDA explicitly perturbs the observations, the model and the boundary conditions, and gives in return estimates of analysis and background error covari-

---

[1] 22.24, 23.04, 23.84, 25.44, 26.24, 27.84, 31.4 GHz

[2] ~~22.24, 23.04, 23.84, 25.44, 26.24, 27.84, 31.4,~~ 51.26, 52.28, 53.86, 54.94, 56.66, 57.3 ~~and~~ , 58 GHz

150 ance ~~(Fisher (2003); Zagar et al. (2005))~~(Fisher, 2003; Zagar et al., 2005). The AROME EDA consists in running an ensemble of 3D-Vars in parallel, where the observations are perturbed according to their prescribed error statistics. The model perturbations are represented by an online multiplicative inflation scheme (Raynaud and Bouttier, 2015). The inflation factor is derived from the skill over spread ratio. The perturbed boundary conditions are taken from the global EDA (Raynaud et al., 2011). The EDA configuration used for this study corresponds to the operational implementation since July 2018 with a horizontal

155 resolution set to $3.2\,$km and an ensemble size of 25 members.

Firstly, using this AROME EDA, a so-called "climatological" **B** was obtained by computing the forecast differences $\epsilon_b^{k,l} = x_b^k - x_b^l$ between members k,l for all grid points of the whole AROME domain and all assimilation cycles on the 28th of October 2016 (IOP1). A specific fog **B** matrix was then computed by applying a fog mask in order to only select grid points for which most of the EDA members forecast fog. According to the discussion on the fog-model predictor used in

160 Ménétrier and Montmerle (2011), the fog mask was based on the presence of liquid water contents above 10^{-6} kg.kg^{-1} in the first three layers of the model. Several fog **B** matrices have been computed using different assimilation cycles. The fog **B** matrix showing the best results in terms of root-mean-square-errors (RMSE) with respect to radiosoundings has then been selected for this study.

Similarly to Brousseau et al. (2016), background error standard deviations are multiplied by a factor $\alpha < 1$ in order to take

165 into account the forecast error reduction while the background range decreases from 3 to 1h (as the AROME EDA provides 3h forecasts whereas the 1D-Var deals with 1h forecasts). Based on comparison with in-situ measurements, an optimal value of $\alpha = 0.7$ was found. This multiplicative factor is only applied on background error standard deviations while cross-correlations are assumed to be the same at the 1 and 3h forecast ranges. Figure 1 compares background error standard deviations for temperature and the natural logarithm of specific humidity computed for the "climatological" and "fog" **B** matrices. Similar

170 shape and magnitude are observed between the two **B** matrices for the natural logarithm of specific humidity. However, in the case of temperature, background errors in fog areas are found to be larger within the first 500 m with a maximum of 0.7 K at 250 m. On the other hand, the "climatological" **B** matrix shows values below 0.5 K within the whole fog layer. Figure 2 shows the cross-correlations between specific humidity and temperature. Similarly to Ménétrier and Montmerle (2011), a strong positive coupling appears in the fog layer within the first 200 m. This coupling implies that a positive temperature error

175 will be translated into a positive specific humidity error (and vice-versa) due to saturated conditions. This structure significantly differs from the one observed in climatological conditions with almost no coupling between the two variables in the boundary layer. The fog layer is also un-coupled with atmospheric layers above the fog top which exhibit a negative coupling between temperature and humidity.

3.2 Optimal configuration of 1D-Var retrievals

The accuracy of 1D-Var retrievals depends not only on the background-error-covariance matrix but also on an adequate specification of the observation-error-covariance matrix. Observation errors are assumed to follow Gaussian distributions with zero mean. A similar method as described in Martinet et al. (2015), De Angelis et al. (2017) and Cimini et al. (2020) has been used to implement a bias correction of BT measurements based on 6-month differences between MWR observations and BTs simu-
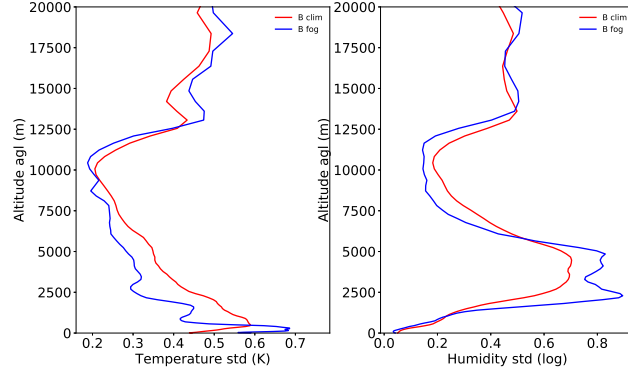
6

Figure 1. Background error standard deviations for temperature (left pannel) and the natural logarithm of specific humidity (right panel) for a "climatological" **B** matrix (red line) or a specific fog **B** matrix (blue line).
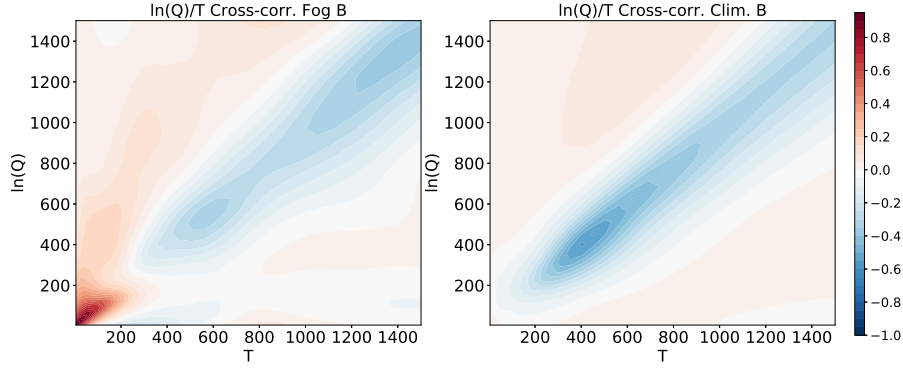

Figure 2. Cross-correlations between the natural logarithm of specific humidity (y-axis) and temperature (x-axis) for a fog **B** matrix (left panel) or a climatological **B** matrix (right panel). x-axis and y-axis are labelled according to altitude above ground in meter.

lated from AROME 1h forecasts with the use of RTTOV-gb (so-called "O-B monitoring"). Table 1 reports the biases obtained for each channel at 90° and the most opaque channels at low elevation angles. The values are consistent with those reported in De Angelis et al. (2017). A static bias-correction of all channels based on table 1 has been applied to the measurements. Observation errors due to liquid nitrogen calibration and spectroscopic errors in radiative transfer models were updated according to recent studies from Maschwitz et al. (2013) and Cimini et al. (2018). Therefore, in addition to commonly used values of instrumental noise (0.5 K for transparents channels and 0.2 K for the most opaque channels), the individual errors defined by

Maschwitz et al. (2013) and Cimini et al. (2018) were added in quadrature:

$$\sigma_{tot} = \sqrt{\sigma_{noise}{}^2 + \sigma_{calib}{}^2 + \sigma_{FM}{}^2}$$

180   with σ_{tot} the total observation errors, σ_{noise} the uncertainty due to noise, σ_{calib} calibration uncertainties and σ_{FM} the uncertainty due to spectroscopic errors in the radiative transfer model. It is important to note that calibration errors of modern MWRs are lower than the ones used in this study due to new developments in the manufacturer software and liquid nitrogen target used for the radiometer calibration. Table 2 summarizes the total observation uncertainty for each channel.

Table 1. Bias of the observation minus background departures computed from AROME forecasts for all frequency at 90° elevation angle and only the most opaque channels (54.94 to 58 GHz) at lower elevation angles.

	22.24	23.04	23.84	25.44	26.24	27.84	31.4	51.26	52.28	53.86	54.94	56.66	57.3	58
90 °	0.41	0.66	0.17	0.18	0.15	-0.43	0.31	-1.30	-4.72	-0.28	-0.04	0.06	0.16	0.20
42 °	-	-	-	-	-	-	-	-	-	-	0.04	0.18	0.22	0.23
30 °	-	-	-	-	-	-	-	-	-	-	0.07	0.24	0.27	0.27
19.2 °	-	-	-	-	-	-	-	-	-	-	0.14	0.31	0.33	0.30
10.2 °	-	-	-	-	-	-	-	-	-	-	0.23	0.37	0.35	0.32
5.4 °	-	-	-	-	-	-	-	-	-	-	0.18	0.24	0.25	0.21

Table 2. Observation uncertainties (K) prescribed in the observation-error-covariance matrix for each channel.

Frequency (GHz):	22.24	23.04	23.84	25.44	26.24	27.84	31.4	51.26	52.28	53.86	54.94	56.66	57.3	58
σ_o (K):	1.34	1.71	1.16	1.08	1.25	1.17	1.19	3.21	3.29	1.30	0.37	0.42	0.42	0.36

    In order to define the best configuration of 1D-Var retrievals in terms of background-error-covariance matrix and bias-correction, statistics have been performed over the 6-month period by comparison with the 120-m tower measurements. For each altitude instrumented with a weather station (50 and 120 m altitude) and each variable (temperature and specific humidity), the error reduction brought by the analysis over the background is defined as:

$$ER = 1 - \frac{RMSE_{xa}}{RMSE_{xb}}$$

with $RMSE_{xa}$ the root-mean-square-errors of the 1D-Var retrieved profiles with respect to the mast measurements, and 185 $RMSE_{xb}$ the root-mean-square-errors of the background profiles with respect to the mast measurements. It is important to note that given the relative low vertical resolution of MWR retrievals, the retrievals at 50 and 120 m are likely to be highly correlated.

Table 4 reports the calculated error reduction for each variable, each altitude and each 1D-Var configuration. The 1D-Var configuration maximizing each ER will be selected as the best configuration. Statistics are divided between fog profiles only 190   (lower part) or all weather-conditions except fog (upper part). In addition to tower measurements limited to only two levels, the

different 1D-Var configurations were also evaluated in terms of bias and RMSE against 21 radiosondes (Figure 3). Radiosondes were launched during IOPs in different atmospheric conditions: the majority are under stratus-cloud and fog conditions and a few of them in clear-sky. Table 3 gives a list of the different configurations evaluated in this section. The three first configu-

195   rations aim at evaluating the impact of the background-error-covariance matrix while the last two configurations focus on the bias-correction.

3.2.1   Sensitivity to the background-error-covariance matrix

In order to evaluate the impact of the background-error-covariance matrix, three experiments have been designed. The CTRL run mimics the configuration of the operational AROME 3D-Var data assimilation system with a "climatological" $\mathbf{B}$ matrix taking into account cross-correlations between temperature and specific humidity. As cross-covariances highly depend on

200   the weather conditions (Hólm et al., 2002; Michel et al., 2011) and the use of fixed covariances is not optimal when dealing with different atmospheric scenarios, Config1 aims at evaluating the impact of the cross-correlations between temperature and humidity on the retrievals. To this end Config1 corresponds to the same configuration but removing the cross-correlations between temperature and specific humidity. It can be noted that this approach is still used in various 3D/4D-Var operational schemes (Barker et al., 2004). Config2 mimics the use of a flow dependent $\mathbf{B}$ matrix during fog conditions only with a full

205   correlated fog-specific $\mathbf{B}$ matrix during fog events but a non-correlated climatological $\mathbf{B}$ matrix for all other weather conditions. For these three configurations, the bias-correction based on clear-sky O-B monitoring is applied to the raw BT measurements.

Table 3. List of 1D-Var experiments.

Expt.	Description	Bias correction (BC)
CTRL	Climatological $\mathbf{B}_{clim}$ matrix computed from the AROME EDA with cross-covariances between T and Q	BC from AROME O-B monitoring
Config1: Bclim NO CROSS CORR	Climatological $\mathbf{B}_{clim}$ matrix computed from the AROME EDA without cross-covariances between T and Q	BC from AROME O-B monitoring
Config2: Bflow dependent	Cross-correlated $\mathbf{B}_{fog}$ matrix if visi_10m < 1000m $\mathbf{B}_{clim}$ without cross-correlations for visi_10m>1000m	BC from AROME O-B monitoring
Config3: Bflow dependent NO BC 54-58 GHz	Cross-correlated $\mathbf{B}_{fog}$ matrix if visi_10m < 1000m $\mathbf{B}_{clim}$ without cross-correlations for visi_10m>1000m	BC from AROME O-B monitoring for channels 22 GHz-53.86 GHz NO BC for channels 54.54 to 58 GHz
Config4: Bflow dependent BC $\delta T < 5K$	Cross-correlated $\mathbf{B}_{fog}$ matrix if visi_10m < 1000m $\mathbf{B}_{clim}$ without cross-correlations for visi_10m>1000m	BC from AROME O-B monitoring base on all clear-sky profiles with T_{500m}-$T_{ground} < 5K$

The worst results are obtained with the CTRL configuration, which considers a "climatological" $\mathbf{B}$ matrix taking into account cross-correlations between temperature and humidity. With this configuration, the specific humidity RMSE with respect

Table 4. Reduction in the RMSE with respect to tower measurements after the 1D-Var analysis ($RMSE_{xa}$) compared to the background ($RMSE_{xb}$) for all weather conditions (upper part) or only fog events (lower part): $ER = 1 - \frac{RMSE_{xa}}{RMSE_{xb}}$ (%). Statistics performed on temperature (T, (K)) and specific humidity (Qspec, kg.kg^{-1}) at 50 and 120 m altitude.

1DVAR / ER	CTRL: $\mathbf{B}_{clim}$ Cross-corr	Config 1: $\mathbf{B}_{clim}$ no cross-corr	Config2: $\mathbf{B}_{fog}\,\mathbf{B}_{clim}$	Config3: $\mathbf{B}_{fog}\,\mathbf{B}_{clim}$ NO BC 56-58 GHz	Config4: $\mathbf{B}_{fog}\,\mathbf{B}_{clim}$ BC ΔT < 5 K
All conditions except fog (statistics on 2534 profiles)					
T 50m	42	42	42	57	54
T 120m	40	40	40	50	50
Qspec 50m	-4	0.2	0.3	0.3	0.3
Qspec 120m	-7	0.1	0.1	0.1	0.1
Fog cases (statistics on 351 profiles)					
T 50m	37	37	34	50	44
T 120m	21	21	24	32	32
Qspec 50m	-7	-1	-5	15	6
Qspec 120m	-20	-3	21	20	21

to tower measurements is degraded by up to 20 % (~~resp.~~ respectively 7 %) at 120 m altitude during fog conditions (~~resp.~~ respectively all weather conditions). This demonstrates the importance of the **B** matrix cross-correlations on 1D-Var accuracy and particularly in the case of observations with low information content on the vertical structure (as MWRs are mainly sensitive to the total column water vapor content due to vertically quasi-constant weighting functions). The humidity profile degradation is significantly reduced to less than 3 % thanks to the use of a block diagonal **B** matrix in Config1. Humidity profiles are finally improved by up to 21 % in RMSE at 120 m during fog conditions with the use of a specific fog **B** matrix adapted to the meteorological conditions. Figure 3 confirms that the best configuration in terms of **B** matrix corresponds to Config2 compared to the CTRL configuration. In fact, the use of a "climatological" **B** matrix with cross-correlations degrades both temperature and humidity retrievals but more significantly specific humidity up to 4 km. Overall, these results confirm that, for MWRs, humidity increments in the lowest levels are significantly driven by the cross-correlations between temperature and humidity. These correlations (sign and amplitude) being highly dependent on the weather conditions, the **B** matrix should ideally be updated for each profile. When it is not possible, the use of a block diagonal **B** matrix might be preferable to avoid degradation in the retrievals due to inaccurate cross-correlations. This result is in line with the study of Dee and Da Silva (2003) which showed that, when humidity is less adequately observed than temperature, it is more accurate to neglect humidity - temperature error covariances. However, when an adapted flow-dependent **B** matrix is used, the specific humidity analysis is improved. In the future, the use of ensemble data assimilation schemes should enable deriving optimal **B** matrices evolving in time and space to be consistent with the weather conditions in order to optimize specific humidity retrievals.

3.2.2 Sensitivity to the bias correction applied on opaque channels

One other source of errors in the lowest levels could come from the bias correction applied on the most opaque channels. In fact, the bias correction has been inferred from differences with respect to the AROME model which is known for larger errors in the boundary layer below 2 km altitude (Martinet et al., 2015, 2017). Two additional configurations have thus been
230 designed to evaluate the impact of the bias correction applied on raw measurements. Config3 is similar to config2 except that the bias-correction is not applied on the last four most opaque channels (54-58 GHz range). Config4 is similar to config2 except that the bias-correction applied to all channels is based on statistics of O-B departures made on clear-sky profiles with a temperature gradient between 500 m altitude and surface smaller than 5 K. Table 4 shows that 1D-Var retrievals are already improved with Config4 in fog conditions. Consequently, removing larger model errors during very stable conditions in the
235 O-B monitoring leads to an improved estimation of the bias correction. The best scores are finally obtained with Config3 with improved temperature retrievals by 15 % at 50 m. Figure 3 confirms that if the bias-correction based on the AROME monitoring is applied to the 54-58 GHz channels, a significant degradation in the temperature retrievals is observed in the first 500 m. Removing the bias correction applied to transparent channels causes a significant degradation of the specific humidity retrievals above 2 km altitude.

240 This result demonstrates that, even though the bias-correction of MWR BT measurements can be computed from AROME short-term-forecasts for transparent channels, this method is not optimal for opaque channels without a thorough screening of the O-B innovations. In fact, the bias-correction of opaque channels depends on the accuracy of the forecast model within the boundary layer, which is known to be degraded during stable conditions. Similar conclusions are found in Martinet et al. (2017), despite the larger period of O-B monitoring (6-months instead of 2-months) and a less complex terrain.

245

Figure 3 finally shows that the best performance is obtained with Config3 through the whole atmospheric column both for temperature and humidity. For temperature, with this best configuration, RMSE smaller than 0.6 K within the fog layer and below 1.6 K considering the whole atmospheric profile up to 6 km altitude are obtained. The 1D-Var analysis outperforms the background in the first 800 m with a maximum improvement observed within the fog layer (RMSE decreased from 2.2 K to
250 0.6 K at 75 m). As expected, most of the information from the MWR observations are located below 2000 m and mainly below 1000 m. For humidity, RMSE accuracies are less than 1 g.kg^{-1} for the best scenario. Most of the improvement brought to the background is located below 3000 m with a maximum RMSE decrease reaching 0.2 g.kg^{-1} at 75 m and 1800 m. Configuration 3 is used in the following sections.

4 Thin radiative fog case study

255 This section focuses on a thin radiative fog case observed on the 28th of October 2016. Figure 4 shows the cloud base height retrieved from a CL31 ceilometer (top panel), the visibility measurements on the instrumented tower at 10 m and 120 m altitude (blue and green lines respectively, middle panel) as well as the 1-hour AROME forecasts of liquid water content (LWC) for the same day (bottom panel). During the whole period, fog is only observed at 10 m altitude during 40 minutes at midnight and
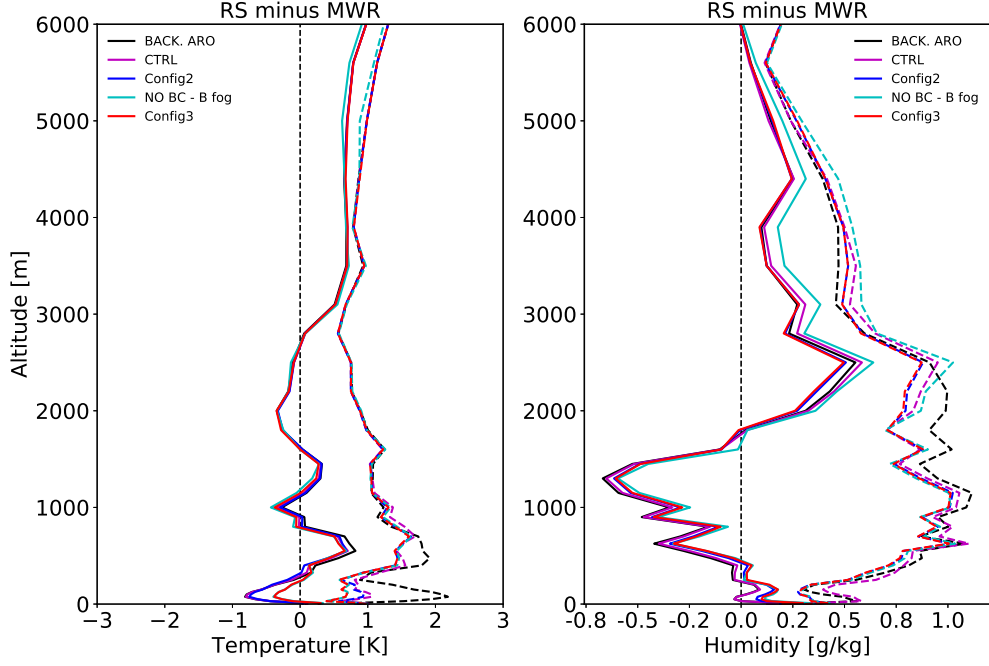
Figure 3. Vertical profiles of (left) temperature and (right) specific humidity bias (solid line) and root-mean-square-errors (dashed lines) of 1D-Var retrievals (coloured lines) and AROME backgrounds (black line) against 21 radiosondes launched during IOPs: 1DVAR retrievals from AROME 1 h forecasts with bias-correction and a cross-correlated climatological **B** matrix (CTRL, magenta), with bias-correction and a cross-correlated dedicated fog **B** matrix (Config2, blue), with bias-correction except channels 11-14 and a cross-correlated dedicated fog **B** matrix (Config3, red), without any bias-correction and a cross-correlated dedicated fog **B** matrix (cyan).

then during 4 hours from 5 to 9 UTC. A stratus-cloud is then observed from 10 UTC until midnight with a cloud base height
260   between 300 and 500 m. The AROME backgrounds simulate a continuous thick fog event from 0 to 13 UTC, which is then lifted until 15 UTC into a stratus cloud at 500 m altitude. The stratus cloud is then dissipated to appear again after 20 UTC. In this example, two main deficiencies in the AROME 1-hour forecasts are observed: a temporally longer and vertically thicker fog event and the erroneous dissipation of the stratus cloud between 15 and 20 UTC.

Figure 5 compares the time series of temperature profiles (top panels) and specific humidity (bottom panels) forecast by
265   AROME (left panels) and retrieved with the 1D-Var scheme using the optimal configuration. We can note the large temperature increment by up to 5 K from 0 to 12 UTC essentially in the first 250 m after 1D-Var is applied; this is the period where the model simulates a thick fog event not confirmed by the observations. This is followed by a temperature cooling within 2 K during the stratus cloud (16 to 24 UTC). The specific humidity is only modified during the fog event (5 to 9 UTC) with an

12

increase of   1 g.kg^{-1} in the first 1500 m.

270   In order to quantify the accuracy of the 1D-Var increments in this specific fog case, Figure 6 evaluates the corresponding diurnal evolution of temperature, specific humidity and relative humidity at 50 and 120 m altitude. A large underestimation of the temperature by 4 to 6 K is observed in the AROME forecasts by night until 13 UTC. AROME forecasts are also found to be too warm by 2 K after 18 UTC. The assimilation of MWR brightness temperatures in a 1D context greatly improves the model background (temperature) during the nightime fog event with temperature errors smaller than 2 K after assimilation.

275 The 1D-Var retrievals almost perfectly fit the in-situ observations after 13 UTC for temperature both at 50 and 120 m altitude. In terms of specific humidity, AROME tends to underestimate the specific humidity at nighttime probably due to an overestimation of the saturation. Indeed, as the fog layer was thicker in AROME than in the observations, we believe the model converts too much water vapour into liquid erroneously, which makes it underestimate specific humidity. On the contrary, the specific humidity is overestimated in the afternoon. After 1D assimilation of MWR measurements, specific humidity is nearly

280 identical to the AROME forecasts except during the longest fog event (between 4 and 9 UTC) where the 1D analysis is closer to the tower measurements than the background. This is likely due to the use of the cross-correlated fog **B** matrix under these conditions as opposite to the use of a block diagonal **B** matrix when fog is not observed. Most of the model increment is thus produced by the **B** matrix cross-covariances. Background errors are reduced from 0.5 g.kg^{-1} to 0.1 g.kg^{-1}. Though closer to the in-situ observations, 1D-Var retrievals slightly overestimate specific humidity between 4 and 9 UTC. This is most likely

285 due to over-estimated positive cross-correlations between temperature and humidity in the **B** matrix. In terms of relative humidity, the temperature warming by night leads to the effect that the fog layer is not saturated any more in agreement with the tower in-situ measurements. However, this field is degraded after 13 UTC. In fact, the 1D-Var scheme correctly reduces the temperature but is not able to decrease the specific humidity. The relative humidity is thus wrongly increased by the 1D-Var analysis.

290   In view of the future inclusion of hydrometeors in the data assimilation control variables, the information brought by MWRs to the liquid water path (LWP) could also be very valuable. Figure 7 shows the time series of LWP forecast by AROME, retrieved through the 1D-Var and retrieved from a quadratic regression applied on BT measurements. It can be seen that the AROME model clearly overestimates the fog LWP with a maximum reaching 90 g.m^{-2} at 7 UTC. This value, however, decreased down to 25 g.m^{-2} after the 1D assimilation of MWR brightness temperatures. During the period where the model

295 fails to simulate the stratus cloud, the LWP is significantly increased in the 1D-Var analysis with values between 30 and 80 g.m^{-2} even if the background profile has no cloud layer between 14 and 20 UTC. These LWP modifications brought by the 1D-Var are consistent with the in-situ observations on the instrumented tower as well as ceilometer observations.

5   Six-month statistics

While the previous section focuses on an extreme fog case, this section aims at more general conclusions on the expected impact

300 of MWR BTs assimilation on AROME analysis. To this end, a statistical evaluation of the expected model increments (analysis minus background differences) after assimilating MWR measurements has been conducted using the tower measurements
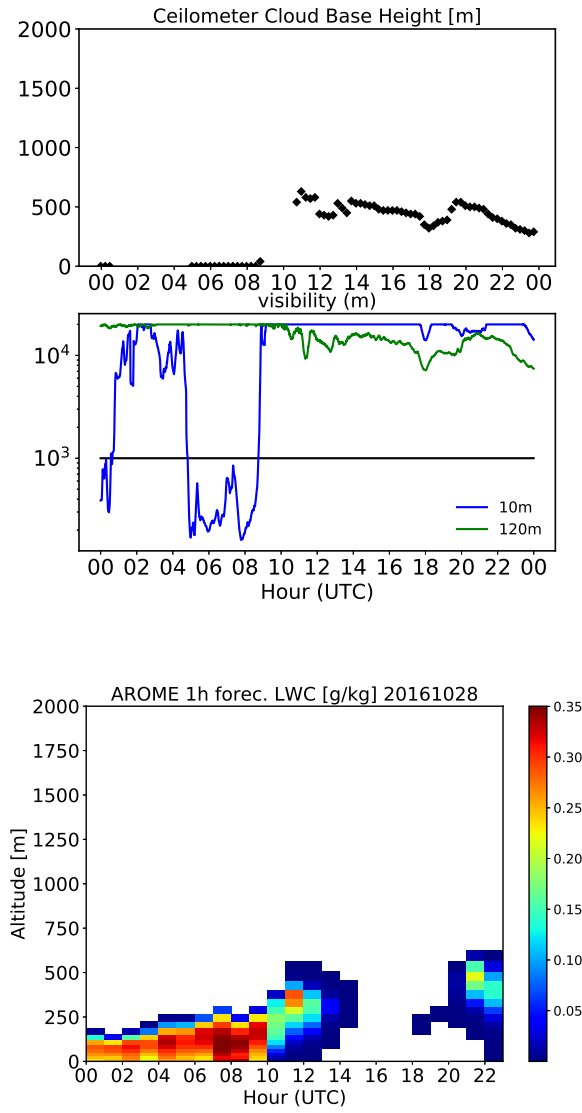
Figure 4. Top panel: Cloud base height (m) derived from the CL31 ceilometer measurements, middle panel: visibility at 10 m (blue) and 120 m (green line), bottom panel: AROME 1-hour forecasts of liquid water content in g.kg^{-1}. 28 October 2016.

during the six-month period. 1D-Var retrievals have been performed using the optimal configuration described in section 3.2. A total of 351 hours of fog (rain events have been removed) could be observed with the MWR. In order to evaluate the performance of the AROME background profiles (1h forecast) to accurately forecast fog events, statistics based on the hit ratio (HR), false alarm rate (FAR), frequency bias index (FBI) and critical-success-index (CSI) have been computed. If GD is the

14
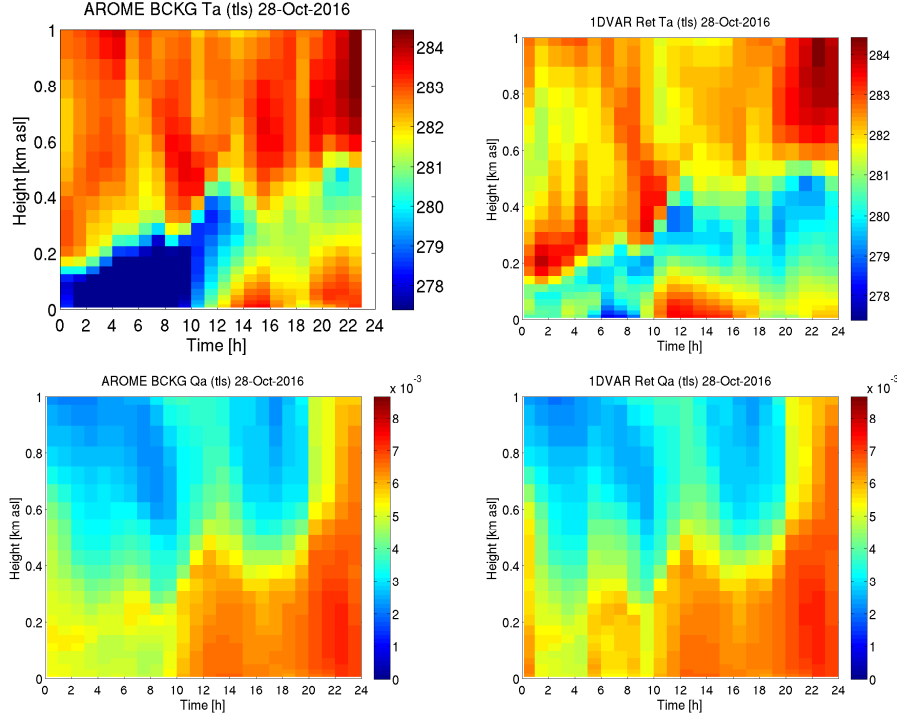
Figure 5. Time series of temperature profiles (top panels) and specific humidity (bottom panels) forecast by AROME (left panels) and retrieved with the 1D-Var scheme with the optimal configuration (Config3, right panels). 28 October 2016.

number of fog profiles well detected, ND the number of undetected fog profiles, FA the number of false alarms, these scores are defined by:

$$
\begin{aligned}
HR &= \frac{GD}{GD + ND} \\
FAR &= \frac{FA}{GD + FA} \\
FBI &= \frac{GD + FA}{GD + ND} \\
CSI &= \frac{GD}{GD + ND + FA}
\end{aligned}
\tag{1}
$$

To detect fog profiles in the model space, a new visibility diagnosis specifically developed for the AROME model has been used (~~Dombrowski-Etchevers et al.~~personal communication, July 2020). In this new diagnosis, the visibility is directly deduced from the liquid water content at ground. It was computed through a statistical regression between hourly maximum of liquid water content forecast by AROME and observed minimum of visibility on 100 ground stations during five months. A hit ratio of 73 % and a false alarme rate of 58 % was found. A FBI of 1.77 means that the AROME background profiles tend to forecast

15

too many fog events. CSI equal to 0.35 means that only 35 % of fog events (observed and/or predicted) are correctly forecast by
the model. These statistics emphasize that quite large errors are observed in the AROME 1h forecasts of fog with an excessive
number of false alarms. In order to evaluate the potential benefit of MWR observations to adjust the AROME background
profiles, the statistical study of model increments is split between the good detections, missed fog profiles and false alarms.

Firstly, the frequency distributions of differences of 1D-Var analysis and background with tower measurements at 50 m
are displayed in Figure 8 both for temperature and specific humidity. For temperature and for all subsets, the distributions
of 1D-Var analysis errors are more centered and more symmetric compared to the background error distributions. Thus, the
largest background errors (above 2 K in absolute values) are succesfully corrected by the 1D-Var analysis. Background error
distributions also present a larger tail towards negative values with a secondary peak centered around -4 K in the case of false
alarms and to a smaller extent in the case of good fog detections. The largest temperature improvement is observed in the case
of false alarms with only 35 % of the background errors being within -0.5 to 0.5 K, against 69 % for the analysis. RMSE with
respect to tower measurements are also significantly improved with values between 1.3 and 1.9 K in the background against
0.6 K in the analysis. The frequency distribution of specific humidity errors for 1D-Var analysis and background are close, with
similar bias and RMSE for good detections and false alarms. A slight degradation is observed for missed fog detections with
a RMSE of 0.33 g.kg^{-1} in the analysis against 0.25 g.kg^{-1} in the background. Overall, the impact on humidity is less evident
than on temperature at 50 m altitude.

To get a vertical perspective, Figure 9 shows the profiles of the frequency distribution of analysis minus background differences.
As more than 90 % of the water vapour increments are within 1 g.kg^{-1} up to 1500 m altitude, only the impact on temperature
is discussed. For each vertical bin, the frequency of the temperature increments within a given range of values is shown. The
frequency distribution of 1D-Var increments has been separated between cases of correct fog detection, missed fog and false
alarms. For all dataset, most of the temperature analysis increments are observed below 750 m and span the range -5 to 5 K.
The largest increments are observed between 100 and 300 m altitude for which around 20 % of the analysis minus background
differences are larger than 2 K in absolute values. We can note significant differences in the shape of the increment distributions
depending on the forecast score. While the distribution of good detections is quite symmetric, it is not the case for missed fog
profiles and false alarm distributions. In the case of missed fog events, the distribution is negatively-skewed close to the ground
whereas it is positively-skewed above 100 m altitude. This asymmetry means that the largest analysis increments in magnitude
tend to decrease the temperature close to the ground and increase the temperature above 100 m. Consequently, we can expect
1D-Var analyses to increase the atmospheric stability in the first 150 m, which is key for fog formation. In the case of false
alarms, the distribution is positively-skewed for all vertical levels. This asymmetry means that the largest analysis increments,
though less frequent in the distribution, occur when the AROME forecasts tend to significantly overestimate the temperature
cooling. By limiting the temperature cooling, the 1D-Var analyses might limit the erroneous saturation leading to false alarms
in the background.

Additional value of MWR data for NWP forecasts and process studies is in the LWP product. In fact, MWR is one of
the most reliable sources for this variable ~~(Crewell and Löhnert (2003))~~(Crewell and Löhnert, 2003), which is key for better
understanding the microphysics of fog lifecycle and limiting the forecast spin-up (i.e. the unbalance of thermodynamic profiles

16

with microphysical variables during the analysis). In fact, as hydrometeors are currently not included in the control variables of
350   most operational variational data assimilation schemes, these fields are kept unchanged during the analysis. Thus, the analyzed
hydrometeor fields correspond to the previous background. Consequently, in the following statistics, the background values
of LWP correspond in fact to the LWP in the operational AROME analysis. These fields are then modified according to the
updated temperature and humidity analyses in the first time steps of the forecast through the model physics. The statistical study
performed here is also useful to evaluate the expected impact on the AROME analyses if MWR observations were assimilated
355   and the LWP included in the control variables. To this end, Figure 10 investigates the frequency distribution of LWP increments
split by forecast skill (good detections, undetected fog, false alarms). Firstly, we can note that the LWP increments are higher
than 50 g.m^{-2} in absolute values for approximately 50 % of good detections and missed fog profiles and 30 % of false alarms.
During false alarms, 95 % of the background LWP values are below 20 g.m^{-2} (not shown), which is close to the MWR
sensitivity which might explain smaller 1D-Var increments during false alarms. The mean increment is the highest in the case
360   of missed fog events (57 g.m^{-2}) and the smallest in the case of false alarms (15 g.m^{-2}). It is important to note that during false
alarms, the LWP increment might be positive due to the presence of cloud layers though we would expect the 1D-Var analysis
to decrease the LWP within the fog layer. If we restrict the statistics to false alarms without cloud aloft, the mean increment
is reduced to -2 g.m^{-2}. As expected, large positive increments occur more often in fog cases un-detected by AROME with
47 % of the distribution showing increments above 50 g.m^{-2} against 35 % in good detections and 22 % in false alarms (8 %
365   for false alarms without cloud layers aloft). To further investigate the LWP increments and retrieved values, more in situ data
are necessary, e.g from the cloud droplet probe mounted on the tethered balloon or cloud radar measurements. However, the
lack of cloud radar measurements to differentiate the LWP within the fog layer and cloud aloft makes this evaluation complex.
Too few cases during which MWR observations were colocated with an entire sounding of the fog layer with the tethered
balloon have been sampled to make an independent evaluation of this product. This is why we use the LWP derived from the
370   MWR alone through a quadratic regression as a reference. The expected accuracy of this product is 15 to 20 g.m^{-2} according
to Crewell and Löhnert (2003). To this end, Figure 12 shows the scatterplot between the LWP retrieved with the MWR alone
(through multi-channel regressions provided by the manufacturer) and the 1D-Var analyses or background profiles (left panel).
We can note the large improvement in correlation between the LWP forecast by the background (0.72) versus the 1D-Var
analysis (0.98) with respect to the MWR multi-channel retrieval. This is of course expected as the 1D-Var minimization tends
375   to get closer to the MWR brightness temperatures which are also used in the multi-channel retrieval. However, this evaluation
is a good sanity check showing the good behaviour of the 1D-Var algorithm and its capability to extract the information from
the observation even with very large errors in the first guess background profiles. The mean error of the AROME LWP is -49
g.m^{-2} and is reduced to -2 g.m^{-2} after 1D assimilation. The root-mean-square-error is significantly reduced from 102 g.m^{-2}
to 27 g.m^{-2}.
380   The same evaluation has been carried out on the IWV (Figures 11 and 12). Since MWRs are more sensitive to column integral
than vertical distribution, more significant impact is expected on IWV than specific humidity profiles. The IWV increments
span from -4 to 4 kg.m^{-2}, which correspond to a change in the background IWV up to 30 %. The distribution of IWV
increments is positively-skewed for correct fog detection meaning that the largest increments in magnitude are observed when

the background underestimates the integrated water vapour content. On the contrary, it is negatively-skewed for missed fog profiles meaning that the largest increments occur when the model overestimates the integrated water vapour content. It is more symmetric in the case of false alarms. The correlation coefficient with respect to the MWR multi-channel retrieval (fig. 12) is sligthly increased from 0.97 to 1. The RMSE is improved from 1.30 to 0.71 $kg.m^{-2}$. The impact of MWR observations is thus positive on IWV, though the good quality of AROME humidity forecast leaves little room for improvement. This could be explained by the assimilation of observations sensitive to the total column water vapor like Global Navigation Satellite System (GNSS) zenith total delay. Further investigation on multiple sites would be needed to confirm this hypothesis.

The next natural step of this study would be to calculate updated scores of fog detections with the new 1D-Var analyses compared to the background profiles. However, forecast scores are only based on the LWC at ground whereas the 1D-Var works on the liquid water path without information on the cloud vertical structure. During false alarms, conclusions on the impact on forecast scores are complexified by the presence of cloud layers above fog in a majority of false alarms which can cause an increase in LWC at ground. As for the hit ratio, it is increased from 73 % in the background to 81 % in the analysis. The rate of missed fog events is also decreased from 27 % in the background to 19 % in the 1D-Var analysis. However, as this evaluation is only based on the LWC change at the ground, it is necessary to evaluate the impact of the new temperature and humidity fields on the LWC after a few time steps of forecasts but this is beyond the scope of this paper. This investigation into the forecast impact will be studied in the future within the framework of the SOFOG3D experiment (section 6).

6   A regional-scale MWR network for fog process studies: the SOFOG3D experiment

This ~~worked~~ study has proved MWRs to be potential good candidates to be assimilated into current mesoscale models with a special focus on fog forecast improvement. However, our conclusions are currently limited by the small dataset (only one winter at one site) and the lack of impact studies on fog forecast. Although, a positive impact is expected on the analysis of the ABL temperature profile and the LWP, and, to a smaller extent, to the IWV, the next step will be to quantify the impact of a more accurate initial state on fog forecast capability. Among the massive number of observations currently assimilated into operational models, the assimilation of only one MWR unit would probably not be efficient to effectively constrain the boundary layer in the model analysis and to keep the valuable information brought by this local observation over the forecast range. In order to go further in this evaluation, the deployment of a dense network of MWRs is necessary to perform a data assimilation study into the operational AROME 3D-Var assimilation system. Thanks to the strong European collaboration built in the framework of the cost action TOPROF (www.cost.eu/COST_Actions/essem/ES1303), pursued by the cost action PROBE (PROfiling the Boundary layer at a European Scale, Cimini et al. (2020)), an un-precedented regional-scale network of 8 MWR units has been deployed in the South West of France during the period October 2019 to April 2020. This network will serve the data assimilation experiment, fog process studies and model evaluation of the international SOFOG3D (SOuth FOGs 3D experiment for fog processes study) experiment led by Météo-France. Figure 13 shows the domain of the dedicated 500 m horizontal resolution AROME version in test for evaluation during SOFOG3D and the location of the 8 MWR units deployed for the experiment. MWR locations have been chosen for an homogeneous spread over the AROME domain at sites

18

known for the high frequency of fog occurrence. An increased density of MWRs is found at the super-site with two co-located
MWRs and a third humidity profiler deployed approximately 7 km away from the super-site to document the impact of surface
heterogeneities on fog characteristics. The methodology introduced in this paper will be extended to the 8 MWRs deployed

420 during SOFOG3D. This large dataset will help quantifying the spatio-temporal variability of fog parameters (thermodynamics
and microphysics) between the different sites, better understand the main processes playing a role in fog formation / dissipation
/ development and run real data assimilation experiments using the operational 3D-Var assimilation scheme of the AROME
model to quantify the expected fog forecast improvement thanks to ground-based MWRs.

7   Conclusions

425 In this study, the expected benefit of ground-based MWRs on NWP analyses during fog conditions has been investigated with
a 1D-Var technique. Temperature, humidity and LWP have been retrieved through the optimal combination of short-term-
forecasts and MWRs brightness temperatures. In this study, a new retrieval algorithm, combining the NWPSAF 1D-Var and
the fast radiative transfer model RTTOV-gb, has been evaluated on a 6-month period spanning 351 hours of fog conditions.
The first part of this work aimed at deriving an optimal background-error-covariance matrix for fog conditions with the use

430 of newly developed AROME EDA. Similarly to Ménétrier and Montmerle (2011), background-error standard deviations were
found to be approximately 40 % larger within the first 250 m for temperature compared to a commonly used "climatological
B matrix". For specific humidity, similar standard deviations were observed. Most of the differences between a climatological
B matrix and a fog **B** matrix were observed in the cross-correlations between temperature and specific humidity, with a strong
positive coupling within the fog layer and uncoupling between the fog layer and atmospheric layers above. The impact of the

435 **B** matrix and bias-correction has been investigated through a statistical evaluation of the retrieval accuracy with respect to the
in-situ measurements on the instrumented tower at 50 and 120 m altitude. The optimal configuration has been defined through
the definition of the error reduction brought by the analysis over the background for each variable (temperature and specific
humidity) and each altitude. The best scenario mimics the use of a "flow dependent" **B** matrix by using a cross-correlated
fog **B** matrix when fog is detected by visibility measurements and an un-correlated climatological **B** matrix during the other

440 conditions. The retrievals of specific humidity at 120 m altitude are the most impacted: contrary to the significant degradation
of the background by around 20 % with a sub-optimal **B** matrix, an improvement of 21% of the background is obtained with an
optimal **B** matrix. This demonstrates the crucial role of the B matrix cross-correlations when assimilating observations with low
information content on the vertical structure. Consequently, the on-going development of an 3D-EnVar scheme for the AROME
model ~~(Montmerle et al. (2018))~~ (Montmerle et al., 2018) is a necessary step to optimally assimilate MWR observations into

445 the AROME model. The use of a static bias-correction based on the monitoring of observation minus background innovations
was also evaluated. Biases of less than 0.5 K were observed for K-band and opaque V-band channels and up to -4.7 K for the
most transparent V-band channels. The found bias is similar to previous studies; its correction applied to BT measurements
improves humidity retrievals above 2000 m but degrades temperature retrievals in the first 200 m. This degradation is most
likely due to well-known larger model errors in the boundary layer during stable conditions, which are incorrectly included in

19

the bias-correction. Restricting the computation of the bias-correction to clear-sky unstable conditions was found to remove most of the degradation. Overall, with the best configuration (flow dependent fog **B** matrix and no bias correction for most opaque channels), temperature and humidity profiles could be retrieved with RMSE below 1.6 K and 1 g.kg^{-1} up to 6 km in the troposphere.

A thin radiative fog sampled during the first IOP of the experiment was then described. For this specific case, the AROME model was found to simulate a temporally longer and vertically thicker fog event and is not able to maintain the stratus cloud in the afternoon. After 1D assimilation of MWR observations, a large warming up to 5 K is observed within the first 500 m during the fog event associated with an increase in specific humidity and a decrease of LWP by 40 to 70 g.m^{-2} consistent with in-situ measurements showing the large impact brought by MWR observations to modify the initial state of the model in fog conditions.

Finally, a statistical evaluation of the expected model increments after assimilating MWR measurements has been conducted using tower measurements. Large forecast errors were observed in the AROME backgrounds with a tendency to overestimate the presence of fog. During missed fog profiles, 1D-Var increments pull towards lower temperature close to the ground and higher temperature above 100 m altitude, i.e. higher atmospheric stability. The largest analysis increments and background errors are observed during false alarms when the AROME forecasts tend to significantly overestimate the temperature cooling. Overall, RMSE values from 1.3 to 1.9 K are observed in the background against 0.6 K in the analysis. For specific humidity, analysis increments are small and below 1g.kg^{-1} within the fog layer. On the contrary, a large impact has been found on the LWP with increments up to 200 g.m^{-2} in extreme missed fog events. A larger impact was found on the IWV than the humidity profile with a RMSE with respect to tower measurements decreased from 1.3 kg.m^{-2} to 0.7 kg.m^{-2} during observed fog profiles. However, it was noted that the AROME backgrounds are more accurate on the IWV compared to temperature and LWP, which leaves less chances for improvement.

Using for the first time the RTTOV-gb fast radiative transfer model, this study investigated the impact of assimilating MWR observations in the AROME model during fog conditions. This evaluation, previously limited to temperature profiles only, was extended to humidity and LWP. Promising results are shown, with significant positive impact on temperature and LWP and small but slightly positive impact on humidity. In order to confirm the results obtained in a 1D-Var framework, the next step is now to assimilate a real network of ground-based MWRs through a 3D-Var or 3D-EnVar data assimilation scheme. Following the recommendations of Caumont et al. (2016) and thanks the strong European collaboration built within the TOPROF and PROBE COST actions, 8 MWRs have been deployed in the South-West of France from October 2019 to April 2020 in the context of the international fog campaign SOFOG3D. The locations of the MWR units have been chosen to optimize their impact in the model specifically for fog forecast evaluation. A 1D-Var plus 3D-EnVar approach will be used to assimilate profiles retrieved through the 1D-Var algorithm presented here, taking the most out of the lessons learnt in this work.

References

Barker, D. M., Huang, W., Guo, Y.-R., Bourgeois, A., and Xiao, Q.: A three-dimensional variational data assimilation system for MM5: Implementation and initial results, Monthly Weather Review, 132, 897–914, 2004.

Bergot, T. and Guedalia, D.: Numerical forecasting of radiation fog. Part I: Numerical model and sensitivity tests, Monthly Weather Review, 122, 1218–1230, 1994.

Bergot, T., Carrer, D., Noilhan, J., and Bougeault, P.: Improved site-specific numerical prediction of fog and low clouds: A feasibility study, Weather and Forecasting, 20, 627–646, 2005.

Brousseau, P., Berre, L., Bouttier, F., and Desroziers, G.: Background-error covariances for a convective-scale data-assimilation system: AROME–France 3D-Var, Quarterly Journal of the Royal Meteorological Society, 137, 409–422, 2011.

Brousseau, P., Seity, Y., Ricard, D., and Léger, J.: Improvement of the forecast of convective activity from the AROME-France system, Quarterly Journal of the Royal Meteorological Society, 142, 2231–2243, https://doi.org/10.1002/qj.2822, http://dx.doi.org/10.1002/qj.2822, 2016.

Caumont, O., Cimini, D., Löhnert, U., Alados-Arboledas, L., Bleisch, R., Buffa, F., Ferrario, M. E., Haefele, A., Huet, T., Madonna, F., and Pace, G.: Assimilation of humidity and temperature observations retrieved from ground-based microwave radiometers into a convective-scale NWP model, Quarterly Journal of the Royal Meteorological Society, 2016.

Cimini, D., Hewison, T. J., Martin, L., Güldner, J., Gaffard, C., and Marzano, F. S.: Temperature and humidity profile retrievals from ground-based microwave radiometers during TUC, Meteorologische Zeitschrift, 15, 45–56, 2006.

Cimini, D., Rosenkranz, P. W., Tretyakov, M. Y., Koshelev, M. A., and Romano, F.: Uncertainty of atmospheric microwave absorption model: impact on ground-based radiometer simulations and retrievals, Atmospheric Chemistry and Physics, 18, 15 231–15 259, 2018.

Cimini, D., Hocking, J., Angelis, F. D., Cersosimo, A., Paola, F. D., Gallucci, D., Gentile, S., Geraldi, E., Larosa, S., Nilo, S., et al.: RTTOV-gb v1. 0–updates on sensors, absorption models, uncertainty, and availability, Geoscientific Model Development, 12, 1833–1845, 2019.

Cimini, D., Haeffelin, M., Kotthaus, S., Löhnert, U., Martinet, P., O'Connor, E., Walden, C., Collaud-Cohen, M., and Preissler, J.: Towards the profiling of the atmospheric boundary layer at European scale – Introducing the COST Action PROBE, Bulletin of Atmospheric Science and Technology, 2020.

Crewell, S. and Löhnert, U.: Accuracy of cloud liquid water path from ground-based microwave radiometry 2. Sensor accuracy and synergy, Radio Science, 38, 7–1, 2003.

De Angelis, F., Cimini, D., Hocking, J., Martinet, P., and Kneifel, S.: RTTOV-gb–adapting the fast radiative transfer model RTTOV for the assimilation of ground-based microwave radiometer observations, Geoscientific Model Development, 9, 2721–2739, 2016.

De Angelis, F., Cimini, D., Löhnert, U., Caumont, O., Haefele, A., Pospichal, B., Martinet, P., Navas-Guzman, F., Klein-Baltink, H., and Dupont, J.-C.: Long-term Observation minus Background monitoring of ground-based microwave radiometer network. Part 1: Brightness Temperatures, Atmospheric Measurement Techniques Discussion, in review, https://doi.org/10.5194/amt-2017-112, 2017.

Dee, D. P. and Da Silva, A. M.: The choice of variable for atmospheric moisture analysis, Monthly weather review, 131, 155–171, 2003.

Dombrowski-Etchevers, I., Seity, Y., Mestre, O., and Willemet, J.-M.: New algorithms for two forecasted products of weather : visibilities and 2 precipitation types, Weather and Forecasting, to be submitted.

Evensen, G.: The Ensemble Kalman Filter: theoretical formulation and practical implementation, Ocean Dynamics, 53, 343–367, 2003.

Fisher, M.: Background error covariance modelling, in: ECMWF Seminar on recent developments in data assimilation for atmosphere and ocean, pp. 45–63, 2003.

Guedj, S., Karbou, F., and Rabier, F.: Land surface temperature estimation to improve the assimilation of SEVIRI radiances over land, Journal of Geophysical Research: Atmospheres, 116, 2011.

Gultepe, I., Tardif, R., Michaelides, S., Cermak, J., Bott, A., Bendix, J., Müller, M. D., Pagowski, M., Hansen, B., Ellrod, G., et al.: Fog research: A review of past achievements and future perspectives, Pure and Applied Geophysics, 164, 1121–1159, 2007.

Hartung, D., Otkin, J., Petersen, R., Turner, D., and Feltz, W.: Assimilation of surface-based boundary-layer profiler observations during a cool- season weather event using an observing system simulation experiment. Part II: Forecast assessment, Mon. Weather Rev, 139, 2327–2346, https://doi.org/10.1175/2011MWR3623.1, 2011.

Hólm, E., Andersson, E., Beljaars, A., Lopez, P., Mahfouf, J.-F., Simmons, A., and Thépaut, J.-N.: Assimilation and Modelling of the Hydrological Cycle: ECMWF's Status and Plans, Tech. rep., ECMWF, 2002.

Hu, H., Zhang, Q., Xie, B., Ying, Y., Zhang, J., and Wang, X.: Predictability of an advection fog event over North China. Part I: Sensitivity to initial condition differences, Monthly Weather Review, 142, 1803–1822, 2014.

Hu, H., Sun, J., and Zhang, Q.: Assessing the impact of surface and wind profiler data on fog forecasting using WRF 3DVAR: an OSSE Study on a dense fog event over North China, Journal of Applied Meteorology and Climatology, 56, 1059–1081, 2017.

Illingworth, A. J., Cimini, D., Haefele, A., Haeffelin, M., Hervo, M., Kotthaus, S., Löhnert, U., Martinet, P., Mattis, I., O'Connor, E., et al.: How Can Existing Ground-Based Profiling Instruments Improve European Weather Forecasts?, Bulletin of the American Meteorological Society, 100, 605–619, 2019.

Lafore, J. P., Stein, J., Asencio, N., Bougeault, P., Ducrocq, V., Duron, J., Fischer, C., Héreil, P., Mascart, P., Masson, V., Pinty, J. P., Redelsperger, J. L., Richard, E., and de Arellano J., V.-G.: The Meso-NH atmospheric simulation system. Part I: Adiabatic formulation and control simulations, in: Annales Geophysicae, vol. 16, pp. 90–109, Springer, 1997.

Löhnert, U. and Maier, O.: Operational profiling of temperature using ground-based microwave radiometry at Payerne: prospects and challenges, Atmospheric Measurement Techniques, 5, 1121–1134, 2012.

Mahfouf, J.-F., Ahmed, F., Moll, P., and Teferle, F. N.: Assimilation of zenith total delays in the AROME France convective scale model: a recent assessment, Tellus A, 67, 26 106, 2015.

Martinet, P., Dabas, A., Donier, J. M., Douffet, T., Garrouste, O., and Guillot, R.: 1D-Var temperature retrievals from microwave radiometer and convective scale model, Tellus A, 67, 27 925, 2015.

Martinet, P., Cimini, D., De Angelis, F., Canut, G., Unger, V., Guillot, R., Tzanos, D., and Paci, A.: Combining ground-based microwave radiometer and the AROME convective scale model through 1DVAR retrievals in complex terrain: an Alpine valley case study, Atmospheric Measurement Techniques, 10, 3385–3402, https://doi.org/10.5194/amt-10-3385-2017, 2017.

Maschwitz, G., Löhnert, U., Crewell, S., Rose, T., and Turner, D.: Investigation of ground-based microwave radiometer calibration techniques at 530 hPa, Atmospheric Measurement Techniques, 6, 2641–2658, 2013.

Mazoyer, M., Burnet, F., Denjean, C., Roberts, G. C., Haeffelin, M., Dupont, J.-C., and Elias, T.: Experimental study of the aerosol impact on fog microphysics, Atmospheric Chemistry and Physics, 19, 4323–4344, 2019.

Ménétrier, B. and Montmerle, T.: Heterogeneous background-error covariances for the analysis and forecast of fog events, Quarterly Journal of the Royal Meteorological Society, 137, 2004–2013, 2011.

Michel, Y., Auligné, T., and Montmerle, T.: Heterogeneous convective-scale background error covariances with the inclusion of hydrometeor variables, Monthly Weather Review, 139, 2994–3015, 2011.

Montmerle, T. and Faccani, C.: Mesoscale assimilation of radial velocities from Doppler radars in a preoperational framework, Monthly Weather Review, 137, 1939–1953, 2009.

Montmerle, T., Michel, Y., Arbogast, E., Ménétrier, B., and Brousseau, P.: A 3D ensemble variational data assimilation scheme for the limited-area AROME model: Formulation and preliminary results, Quarterly Journal of the Royal Meteorological Society, 144, 2196–2215, https://doi.org/10.1002/qj.3334, 2018.

Otkin, J., Hartung, D., Turner, D., Petersen, R., Feltz, W., and E, J.: Assimilation of surface-based boundary layer profiler observations during a cool-season weather event using an observing system simulation experiment. Part I: Analysis impact, Monthly Weather Review, 139, 2309–2326, https://doi.org/10.1175/2011MWR3622.1, 2011.

Pergaud, J., Masson, V., Malardel, S., and Couvreux, F.: A parameterization of dry thermals and shallow cumuli for mesoscale numerical weather prediction, Boundary-layer meteorology, 132, 83–106, 2009.

Philip, A., Bergot, T., Bouteloup, Y., and Bouyssel, F.: The impact of vertical resolution on fog forecasting in the kilometric-scale model arome: a case study and statistics, Weather and Forecasting, 31, 1655–1671, 2016.

Pinty, J. and Jabouille, P.: A mixed-phase cloud parameterization for use in mesoscale non-hydrostatic model: simulations of a squall line and of orographic precipitations, in: Conf. on Cloud Physics, pp. 217–220, Amer. Meteor. Soc Everett, WA, 1998.

Raynaud, L. and Bouttier, F.: Comparison of initial perturbation methods for ensemble prediction at convective scale, Quart. J. Roy. Meteorol. Soc., 142, 854–866, 2015.

Raynaud, L., Berre, L., and Desroziers, G.: An extended specification of flow-dependent background error variances in the Météo-France global 4D-Var system, Quarterly Journal of the Royal Meteorological Society, 137, 607–619, https://doi.org/10.1002/qj.795, http://dx.doi.org/10.1002/qj.795, 2011.

Rodgers, C. D.: Inverse methods for atmospheric sounding: theory and practice, vol. 2, World scientific, 2000.

Rose, T., Crewell, S., Löhnert, U., and Simmer, C.: A network suitable microwave radiometer for operational monitoring of the cloudy atmosphere, Atmospheric Research, 75, 183–200, 2005.

Seity, Y., Brousseau, P., Malardel, S., Hello, G., Bénard, P., Bouttier, F., Lac, C., and Masson, V.: The AROME-France convective-scale operational model, Monthly Weather Review, 139, 976–991, 2011.

Tav, J., Masson, O., Burnet, F., Paulat, P., Bourrianne, T., Conil, S., and Pourcelot, L.: Determination of Fog-Droplet Deposition Velocity from a Simple Weighing Method, Aerosol and Air Quality Research, 18, 103–113, 2018.

Vandenberghe, F. and Ware, R.: 4-dimensional variational assimilation of ground-based microwave observations during a winter fog event, in: Proceedings International Symposium on Atmospheric Sensing with GPS, Tsukuba Japan, 2002.

Wattrelot, E., Caumont, O., and Mahfouf, J.-F.: Operational implementation of the 1D+ 3D-Var assimilation method of radar reflectivity data in the AROME model, Monthly Weather Review, 142, 1852–1873, 2014.

Zagar, N., Andersson, E., and Fisher, M.: Balanced tropical data assimilation based on a study of equatorial waves in ECMWF short-range forecast errors, Quarterly Journal of the Royal Meteorological Society, 131, 987–1011, https://doi.org/10.1256/qj.04.54, http://dx.doi.org/10.1256/qj.04.54, 2005.
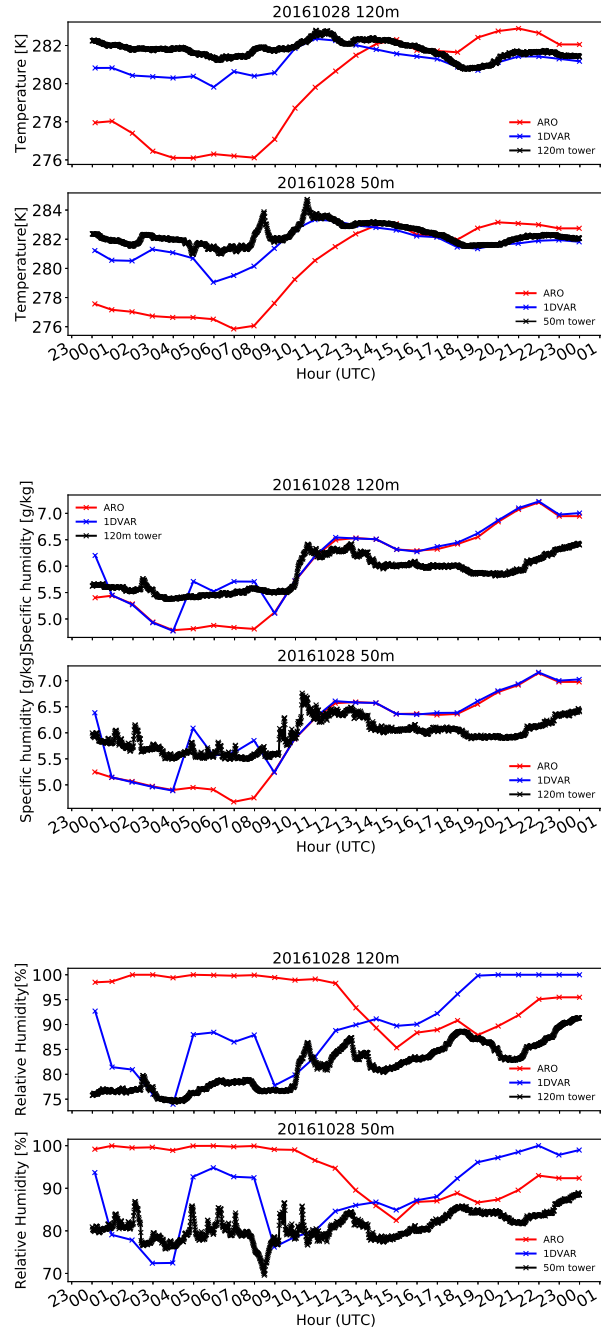
Figure 6. Diurnal evolution of temperature (top panel), specific humidity (middle panel) and relative humidity (bottom panel) forecast by AROME (red), measured by weather station (black) and retrieved by the 1D-Var algorithm (blue). 28 October 2016.
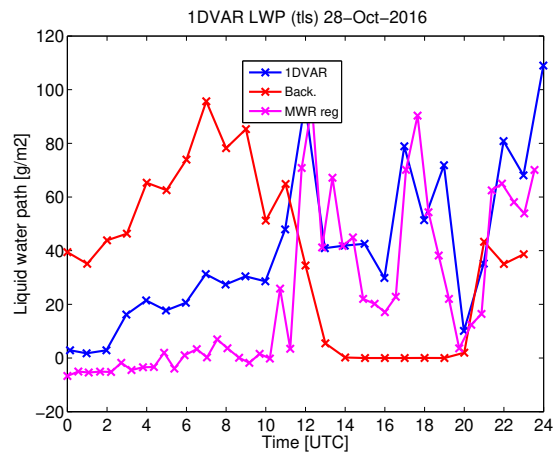
Figure 7. Time serie of liquid water path forecast by AROME (red), retrieved by the 1D-Var algorithm (blue) or retrieved from the MWR alone through a quadratic regression (magenta). 28 October 2016.
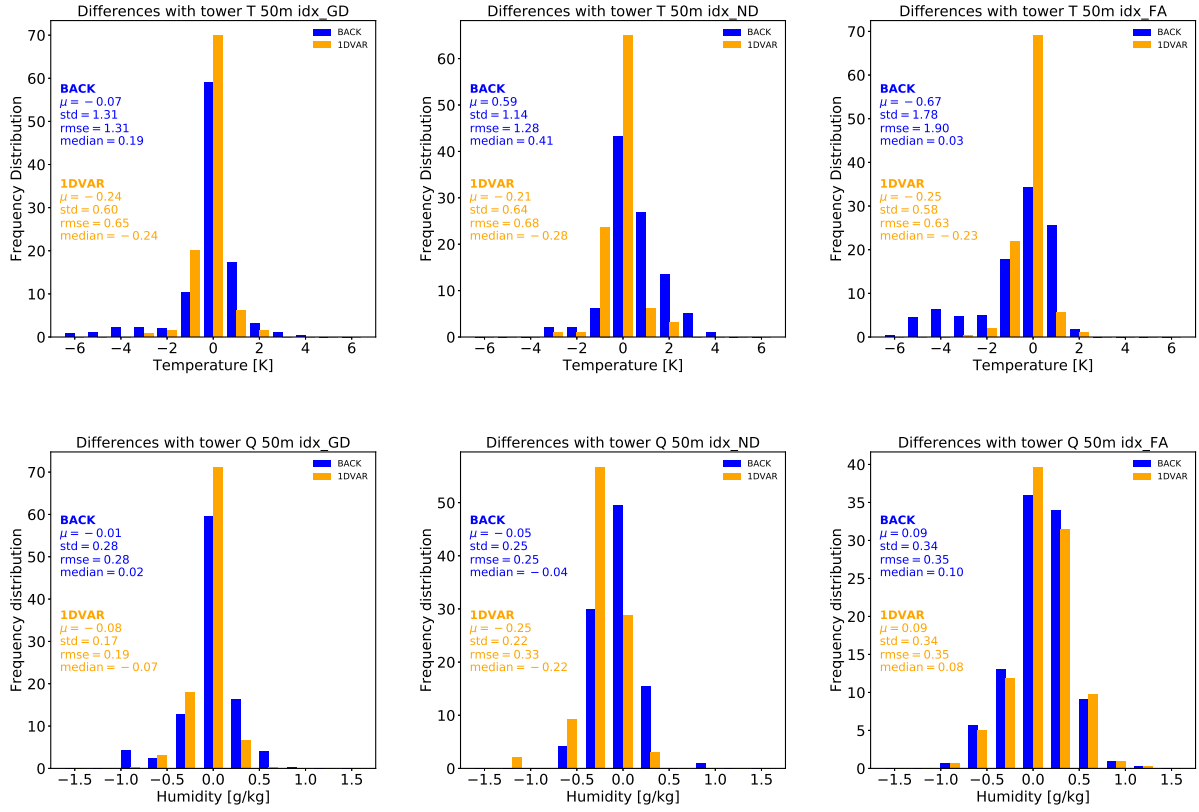
Figure 8. Frequency distribution of 1D-Var analyses (orange) and background (blue) differences compared to tower measurements for temperature (top panel) and specific humidity (bottom panel) at 50 m altitude. Statistics performed over 255 profiles of good fog detection (left panel), 95 profiles of undetected fog (middle panel) and 368 profiles of false alarms (right panel).
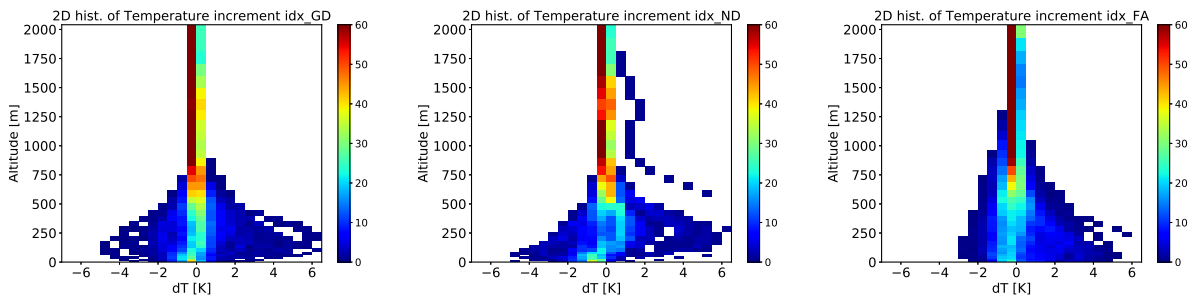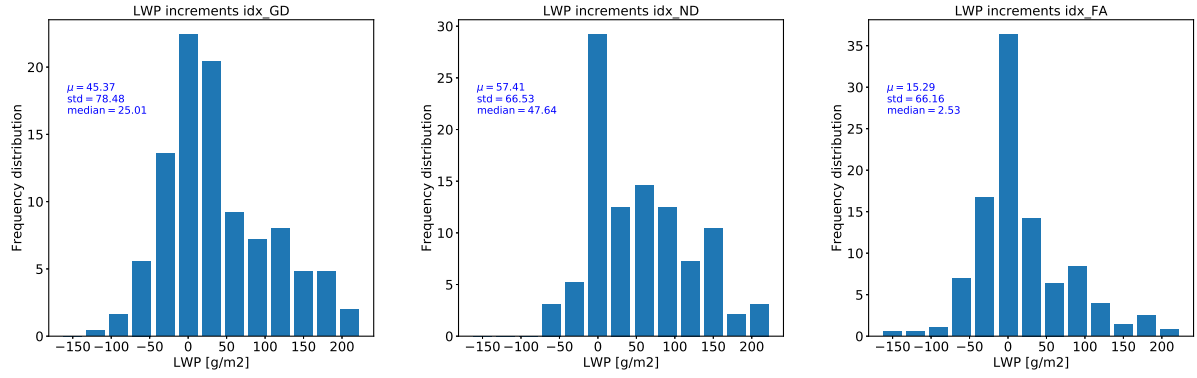

Figure 9. Vertical profiles of the frequency distribution of temperature increments (analysis minus background differences). Statistics performed over 255 profiles of good fog detection (left panel), 95 profiles of undetected fog (middle panel) and 368 profiles of false alarms (right panel).
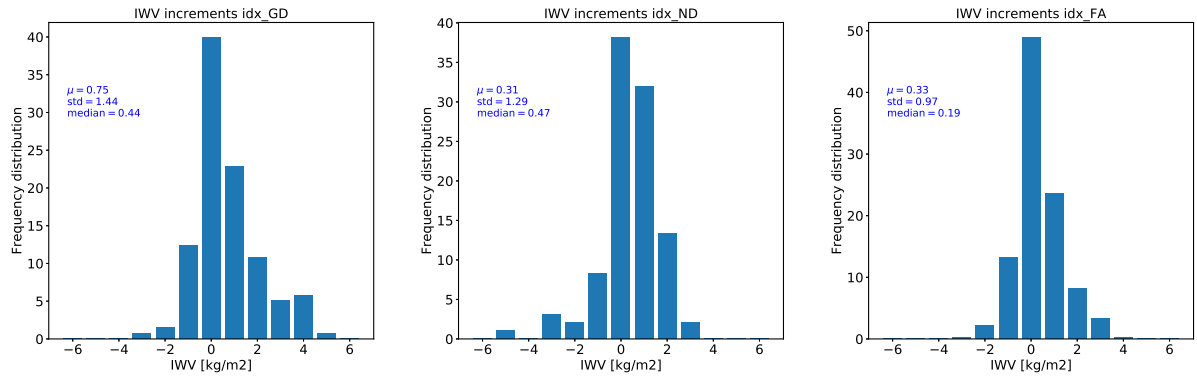
Figure 10. Frequency distribution of 1D-Var LWP increments (g.m^{-2}). Statistics performed over 255 profiles of good fog detection (left panel), 95 profiles of undetected fog (middle panel) and 368 profiles of false alarms (right panel).

Figure 11. Frequency distribution of 1D-Var IWV increments (kg.m^{-2}). Statistics performed over 255 profiles of good fog detection (left panel), 95 profiles of undetected fog (middle panel) and 368 profiles of false alarms (right panel).
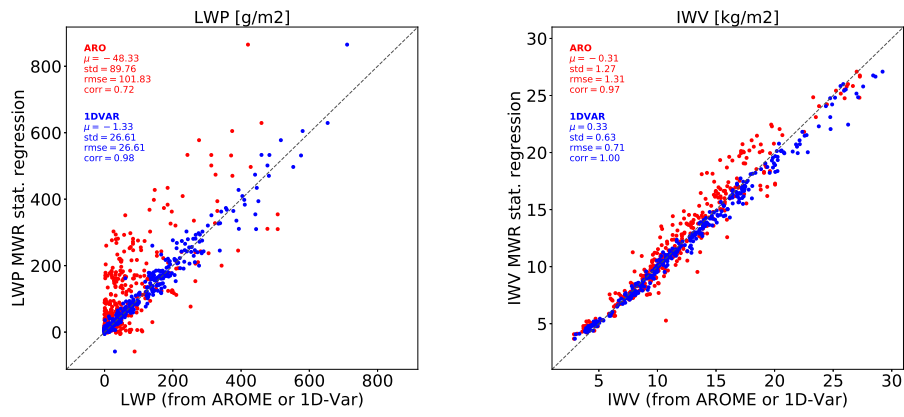
Figure 12. Scatterplot between a multi-channel regression based on MWR observations (y-axis) and the background forecast by AROME (red dots) or the 1D-Var analysis (blue dots) for LWP (left panel) and IWV (right panel). Statistics performed over 351 observed fog profiles.
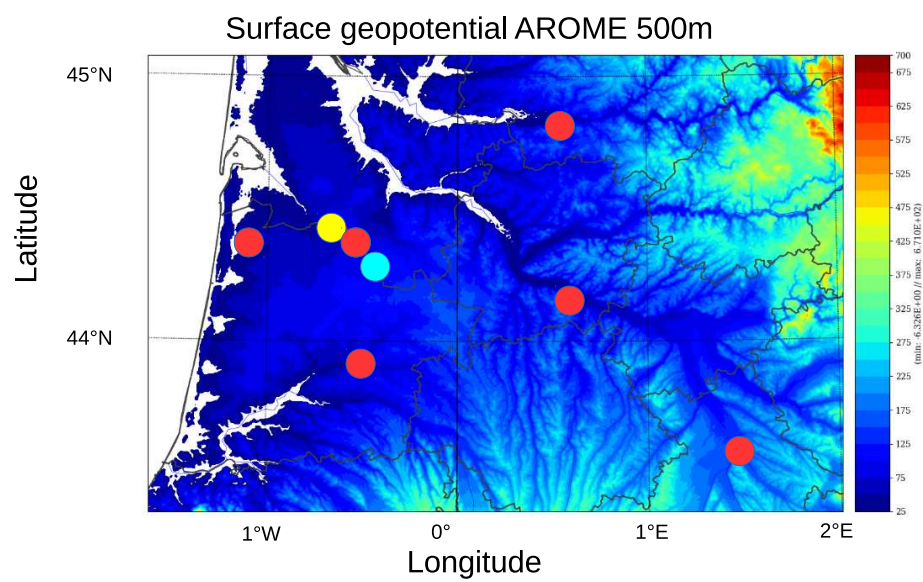
Figure 13. Surface geopotential and domain of the AROME-500m dedicated to the SOFOG3D experiment. Locations of the MWR sites are shown with the filled circles (red indicate temperature and humidity profilers, yellow only humidity retrievals and cyan only temperature retrievals.)